

Analysis of the high-frequency response of atomic force microscope cantilevers

U. Rabe, J. Turner*, W. Arnold

Fraunhofer Institut für zerstörungsfreie Prüfverfahren (Izfp), Universität, Geb. 37, D-66123 Saarbrücken, Germany
 (Fax: +49-681-30693, Email: rabe@izfp.fhg.de)

Received: 25 July 1997/Accepted: 1 October 1997

Abstract. In most commercial atomic force microscopes, dynamic modes are now available as standard operation modes. Acoustical vibrations of atomic force microscope cantilevers can be excited either by insonification of the sample or by vibration of the clamped cantilever end. The resulting dynamical system is complex and highly nonlinear. Simplification of this problem is often realized by modeling the cantilever as a one-degree-of-freedom system such that the higher-order flexural modes are neglected. This point-mass model has been successful in advancing material property measurement techniques. The limits and validity of such an approximation have not been fully addressed. In this paper, the flexural beam equation is examined and compared with the point-mass model by using analytical and finite difference numerical techniques. The two systems are shown to have differences in drive-point impedance and are influenced differently by the surface damping and the contact stiffness. The angular deflection at the end of the beam and the influence of lateral sensor tip motion are considered. It is shown that the higher modes must be included for excitations above the first resonance if both the low- and the high-frequency dynamics are to be modeled accurately.

added. In many applications (for example topography imaging of soft surfaces which might be deformed by the forces applied by the sensor tip), dynamic modes have even replaced the contact force and friction mode. But dynamic modes are not only interesting because they supply topography information with less surface damage than the contact mode. They can also provide additional image contrast on sample surface properties, for example stiffness or adhesion. This has been demonstrated for example by the various atomic force acoustic modes [6–8]. The range of mechanical vibration frequencies which are used for AFM imaging covers acoustic vibrations (up to 20 kHz) and ultrasonic frequencies from 20 kHz up to the MHz range.

1 Linear models

To interpret dynamic AFM images a theoretical description of the vibrating tip-sample system is necessary. Figure 1 shows the situation in an AFM. The cantilever is a small elastic beam with a length of 100–400 μm and a few μm thickness. One end of the cantilever is clamped. The length of the sensor tip at the free end is typically 4–15 μm . The sensor tip is in force interaction with the sample surface. Flexural vibrations can be excited in the cantilever by vibrating the clamped end or vibrations can be coupled into the cantilever by excitation of the sample surface, as in some types of atomic force acoustic microscopy [6, 7].

In the rectangular beam model (Fig. 2b), the cantilever is a three-dimensional continuum with width a , height b and length L . Its material density and Young's modulus are ρ and E , respectively. x is the coordinate along the cantilever and $y(x, t)$ is the deflection of a length element from its rest position. The sensor tip is assumed to be exactly at the end of the beam at $x = L$, though this is not the case for most commercial beams. The equation of motion for flexural vibrations in a beam with uniform cross-section is a partial differential equation of fourth-order [9, 10].

The earliest publications on atomic force microscopy (AFM) suggested dynamic modes in which the small microfabricated cantilever vibrates at higher frequencies compared with the tip-sample scanning frequency [1, 2]. Originally these methods were used to increase the force sensitivity in non-contact AFM, as, for example, in magnetic force microscopy [3]. Within the last years, dynamic modes became more widespread and are now available as standard operation modes in most commercial instruments. New dynamic modes (for example the intermittent contact or tapping mode [4] and the force modulation mode [5], where the vibrating cantilever is in repulsive contact with a sample surface) have been

* Present address: Department of Engineering Mechanics, 212 Bancroft Hall, University of Nebraska-Lincoln, Lincoln, NE 68588-0347, USA

$$EI \frac{\partial^4 y}{\partial x^4} + \eta_{\text{air}} \rho A \frac{\partial y}{\partial t} + \rho A \frac{\partial^2 y}{\partial t^2} = 0 \quad (1)$$

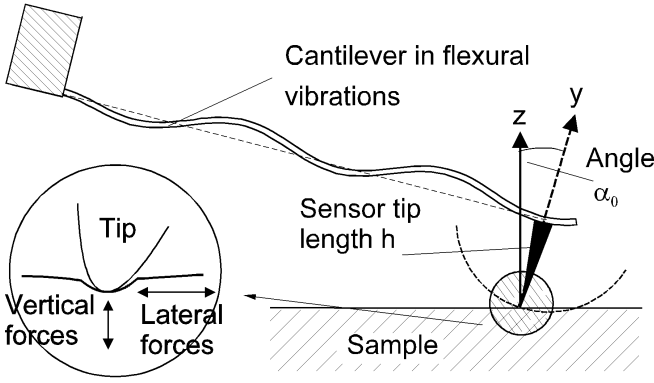


Fig. 1. The cantilever is a small elastic beam with 100–400 μm length and a few μm thickness. In most AFMs it is tilted about 15° relative to the sample surface. This means that the forces F applied to the sample surface have a component vertical to the surface and a lateral component. Typical sensor tip heights h are 4–10 μm . The lower end of the sensor tip undergoes a circular motion when the cantilever vibrates

Here, $I = ab^3/12$ is the area moment of inertia and η_{air} is a damping constant. This equation is solved by considering the boundary conditions of the beam. When the sensor tip is not in contact with a sample surface, the situation of a clamped-free cantilever arises, which is well known. One obtains a characteristic equation. The solutions $k_n L$ of this equation define an infinite set of flexural modes with wavenumbers $k_n = 2\pi/\lambda_n$, $\{n = 1, 2, \dots\}$, where n is the mode number and λ_n the acoustic wavelength of the n th mode. The resonance frequencies $\omega_n = 2\pi f_n$ are obtained using the dispersion relation for flexural waves in a beam:

$$k_n = \sqrt{\omega_n} \cdot \sqrt[4]{\frac{\rho A}{EI}} \quad (2)$$

The stiffness $k_c = 3EI/L^3$ of the beam is calculated from the static deflection of the beam when a force acts at $x = L$.

The complexities of the elastic beam vibrations have given rise to models that simplify the dynamics considerably. In one such approach the elastic beam equation is approximated by a one-degree-of-freedom mass-spring model. In this point-mass model, or first mode approximation (FMA), the cantilever is regarded as a harmonic oscillator consisting of a point mass m^* with a massless spring with stiffness k_c and one resonance frequency $\omega_0 = \sqrt{k_c/m^*}$, as shown in Fig. 2a. The motion of the end of the beam, $y(L, t)$, is represented by the motion of the point-mass $d(t)$. The effective mass in the point mass model m^* is chosen such that the first flexural vibration frequency ω_1 of the free beam equals the point-mass resonance frequency $\omega_0 = \sqrt{k_c/m^*}$:

$$m^* = \frac{k_c}{\omega_1^2} = \frac{3\rho LA}{(k_1 L)^4} \quad (3)$$

$k_1 L \approx 1.875$ is the wavenumber of the first clamped-free flexural mode times the length of the beam.

Damping in the free cantilever is mainly due to friction with air and radiation of sound into the air. In the beam model, air damping is introduced into the differential equation by

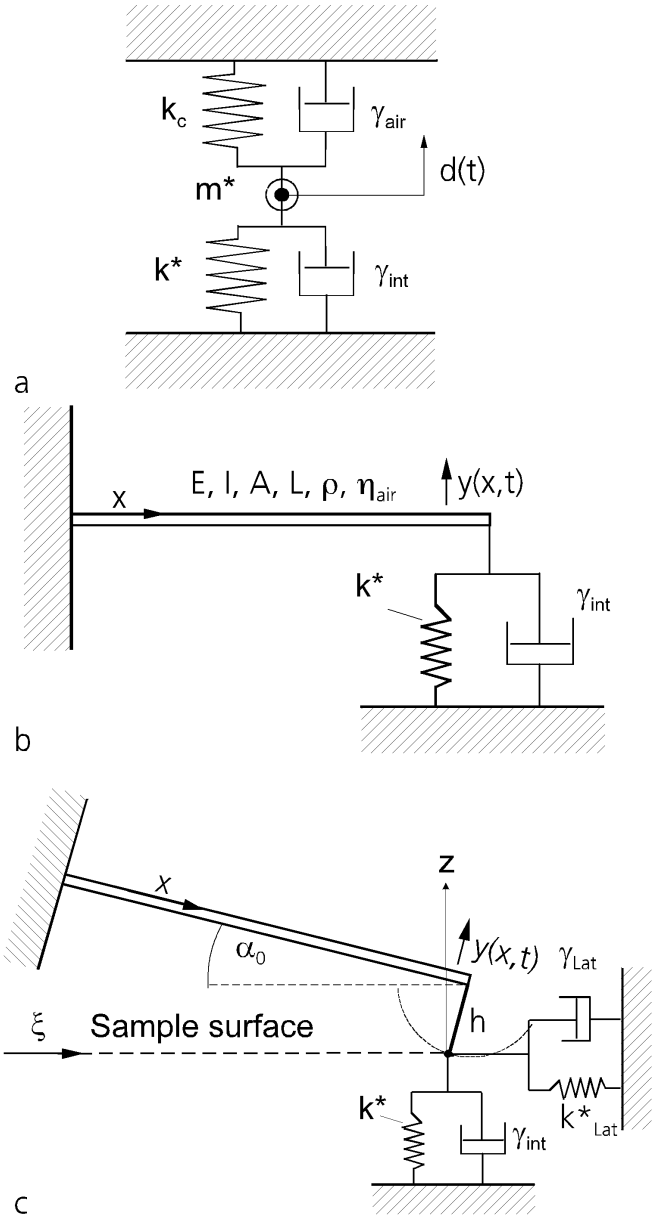


Fig. 2. **a** Point-mass model; **b** elastic beam model; **c** elastic beam model taking into account lateral forces. The tip-sample interaction forces are modeled by the contact stiffnesses k^* and k_{Lat}^* and by the dashpots γ_{int} and γ_{Lat}

the term proportional to the velocity of the length elements, $\eta_{\text{air}} \rho A \partial y / \partial t$. This term makes the wavenumber k complex, which means that the acoustic wave traveling through the beam loses energy. With this damping term, the Q -value of the resonances becomes $Q = \omega_n / \Delta\omega = \omega_n / \eta_{\text{air}}$ for the free beam in air. $\Delta\omega$ is $1/\sqrt{2}$ of the width of the amplitude resonance peak and can be measured experimentally. Typical Q -factors of the first resonances of free AFM cantilevers range from 200 to 600 in air [10]. However, η_{air} is not a constant in most cases, but a function of frequency [11]. In the point-mass model the air damping is represented by the dashpot γ_{air} , yielding a Q -value of the free point-mass resonator, $Q = m^* / \gamma_{\text{air}}$.

When the cantilever tip is near the sample surface, an attractive and repulsive force interaction between the sensor tip and the surface occurs. It is well known that these forces

(for example van der Waals forces, electrostatic forces, adhesion or contact forces) are a highly nonlinear function of tip-sample separation. Only for very small tip-sample vibration amplitudes can they be approximated by a linear spring k^* , shown in Figs. 2a–c; i.e. the forces $F(z)$ perpendicular to the sample surface can be expressed by the partial derivative of F with respect to z in the setpoint position z_e , $k^* = -\partial F/\partial z(z = z_e)$. Though the validity of this linear model is limited, it is helpful for understanding the cantilever-surface interaction. In principle, all interaction forces contribute to the contact stiffness k^* . We used the Hertzian model [12] to calculate a rough estimate of k^* for a cantilever vibrating in contact with a sample surface [10]. For a sharp silicon sensor tip with a radius of 10 nm on a PMMA surface with a Young's modulus of 3×10^{-9} N/m² and an adhesion force of 10^{-8} N for example, one obtains $k^* \approx 20$ N/m. For a blunt silicon tip with a radius of 50 nm on a steel surface (Young's modulus $(2 \times 10^{11}$ N/m²) and an adhesion force of 10^{-7} N one obtains $k^* \approx 600$ N/m. Apart from elastic forces, there can be energy losses due to the motion of the tip relative to the surface. In the models presented here, only losses proportional to the tip-sample velocity are present as dashpots γ_{int} .

When the cantilever is in flexural vibrations, the free end of the cantilever and the sensor tip vibrate at an amplitude $y(L, t)$. Additionally, a time-dependent angular deflection $\alpha(L, t) = \partial y(x, t)/\partial x$ arises. Since the sensor tip is of finite length, its lower end undergoes circular motion, as indicated in Figs. 1 and 2c. This means that not only vertical forces but also lateral tip-sample forces constrain the cantilever motion. In most AFMs the cantilever is inclined at an angle α_0 of about 15° relative to the sample surface. A cantilever force F applied in the y -direction therefore has a component vertical to the sample surface and a small component parallel to the sample surface; i.e. the (ξ, z) -coordinate system of the sample surface is rotated relative to the cantilever (x, y) -coordinate system, and vice versa. To consider lateral forces and the inclination of the cantilever, a second spring-dashpot system parallel to the sample surface was added, as can be seen in Fig. 2c. Though k_{lat}^* and γ_{lat} are again nonlinear functions of ξ and also of z , as a first step only a linear force interaction is studied here. When the cantilever is parallel to the sample surface ($\alpha_0 = 0$), a small angular deflection of the beam end of $\alpha(L, t)$ causes a translation $\alpha(L, t)h$ of the sensor tip on the sample surface, which gives rise to a restoring force $F_{\text{lat}} = -k_{\text{lat}}^* \alpha h$ from the lateral spring. Because of the length of the sensor tip h , a moment $M = -h F_{\text{lat}} = -k_{\text{lat}}^* \alpha h^2$ acts on the end of the cantilever. The effect of the lateral spring fixed to the lower end of the sensor tip is that of a torsional spring fixed to the end of the beam [13]. The moments from the torsional spring can be included in one of the boundary conditions of the cantilever. The characteristic equation and the solutions for a vibration forced by vibrating the clamped end are given in the appendix.

One important distinction between the elastic beam equation and the FMA is the difference in their drive-point impedance, defined as the ratio of the system velocity at a particular location to the force applied at the same location. The drive-point impedance provides a sense of how much energy the beam is willing to accept from an excitation at a particular frequency. The point-mass model takes into account only the fundamental flexural mode of the cantilever and of course cannot predict the high impedances that occur at the higher

resonances. However, as has been shown recently [14], the FMA underestimates the drive-point impedance at the end of the beam ($x = L$) for all frequencies higher than the first mode, even away from resonance. As will be shown now, this effect is even more pronounced when forced vibrations excited at the clamped end of the cantilever are compared.

Figures 3a–c show a comparison between the forced vibrations calculated from the different models. A vibration amplitude of the clamp of $a(t) = a_0 e^{i\omega t}$ was assumed. $f = \omega/2\pi$ is the excitation frequency. The dotted lines show the normalized amplitudes calculated from the point-mass model $|d(\omega)|/a_0$, the dashed lines show the amplitudes calculated from the beam model, $|y(L, \omega)|/a_0$, and the full lines show the normalized slope $|\alpha(L, \omega)| \cdot L/(1.5 \cdot a_0)$. The amplitude or slope axis is displayed in logarithmic scale. The frequency axis was normalized to $f_0 = \omega_0/2\pi$, i.e. the first resonance frequency of the clamped-free undamped beam.

Figure 3a shows vibration spectra for the free beam without tip-sample forces ($k^* = k_{\text{lat}}^* = \gamma_{\text{int}} = \gamma_{\text{lat}} = 0$). The first three resonance frequencies of the beam can be seen. Their position is marked by the dashed vertical lines. a Q -value of 200 was chosen for the first resonance frequency, and η_{air} was assumed to be a constant. Figures 3b and c show the vibration spectra for a beam in linear force interaction with the sample surface. In Fig. 3b $k^*/k_c = 20$ and in Fig. 3c $k^*/k_c = 200$ were chosen, respectively. The interaction damping was small, i.e. the dimensionless damping constant defined in the appendix was $p = 0.01$. As can be seen from the figures, the spectral position of all beam resonances shifts to higher values, but within a fixed range. A given contact stiffness does not affect all modes in the same way. The amplitudes predicted by the point-mass model are orders of magnitude too small and the resonance frequencies predicted for the first mode are too high.

Optical beam deflection sensors are very common as position sensors in AFM. The signal they produce is proportional to the angular deflection (the slope) $\alpha(x, t) = \partial y(x, t)/\partial x$ at the end ($x = L$) of the cantilever. For static deflections the amplitude at the end of the beam $y(L, t)$ is proportional to the slope: $y(L, t) = (L/1.5) \partial y/\partial x(x = L, t)$. However, for a cantilever vibrating near or above its resonance frequency, this relation no longer holds, as can be seen by comparing the dashed and solid lines in Figs. 3a–c. If, for example, the cantilever was pinned at $x = L$, its vibration amplitude would be zero at $x = L$, although the angular deflection $\alpha(x, t)$ need not to be zero because a cantilever can still vibrate between a pinned and a clamped end.

Figure 3d shows the influence of the lateral forces on the slope spectrum. The vertical contact stiffness was the same as in Fig. 3c, and the thin solid line shows the same slope spectrum as in Fig. 3c ($k^*/k_c = 200$, $k_{\text{lat}}^* = 0$, $\alpha_0 = 0$). The thick full line shows the spectrum for the case when lateral stiffness is included ($k^*/k_c = 200$, $k_{\text{lat}}^* = 0.85k^*$, $\alpha_0 = 0$) and the dashed line shows the case when the inclination of the cantilever is also included ($k^*/k_c = 200$, $k_{\text{lat}}^* = 0.85k^*$, $\alpha_0 = 15^\circ$). The resonances shift to higher frequencies when the lateral forces are considered and the slope at the end decreases, because for infinite lateral forces the cantilever would be fixed and the slope would go to zero. When the inclination of the cantilever is changed from 0° to 15° the frequencies decrease a little because the lateral stiffness is assumed to be smaller than the vertical stiffness. Though the changes of frequency

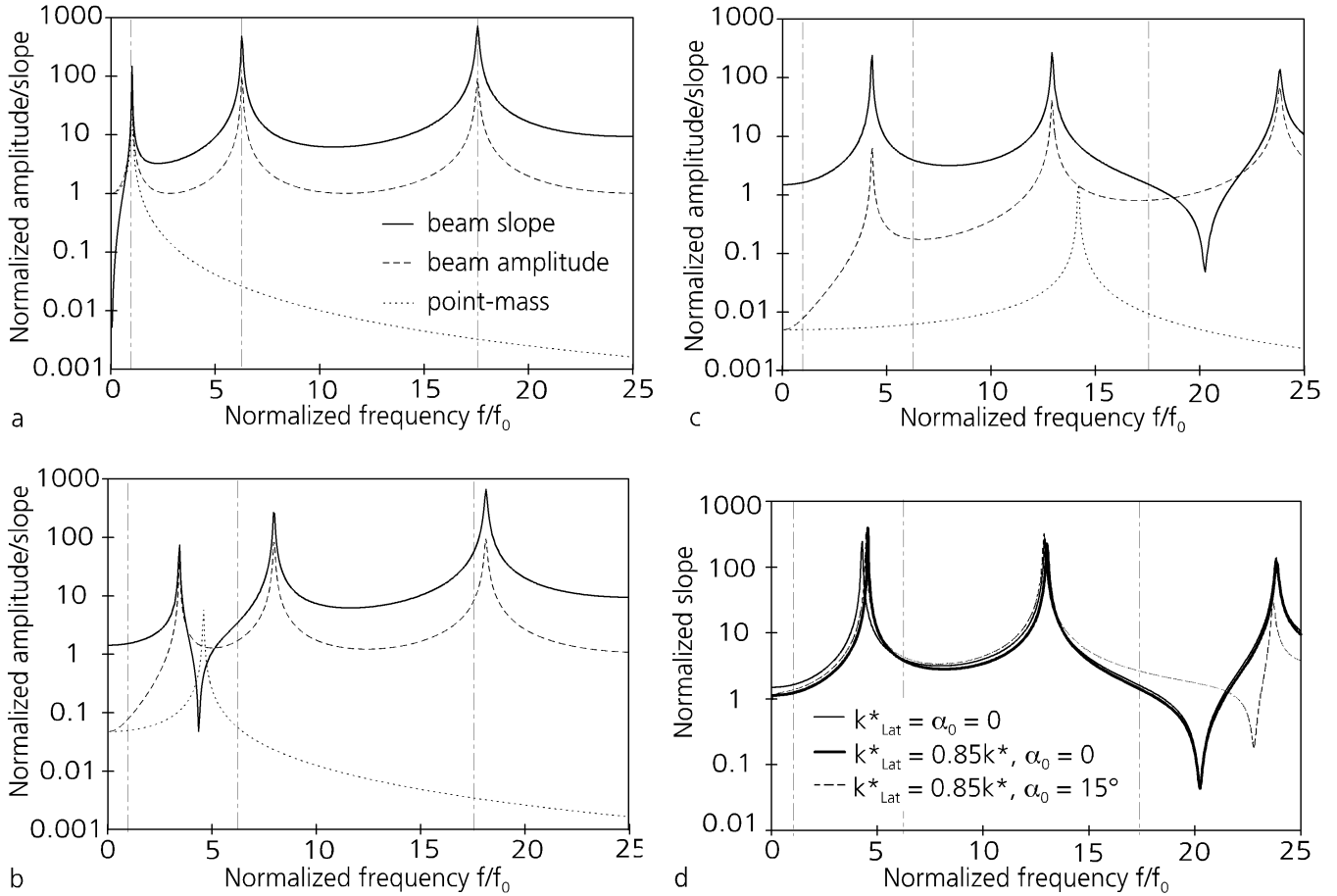


Fig. 3a–d. Forced vibration amplitude of the cantilever deflection (dashed line) and the cantilever slope (solid line) compared with the point-mass model (dotted line). **a** Clamped-free cantilever: $k^* = k_{\text{Lat}}^* = \gamma_{\text{int}} = \gamma_{\text{Lat}} = 0$. **b** Soft surface: $k^*/k_c = 20$, small interaction damping γ_{int} ($p = 0.01$), no lateral forces, $k_{\text{Lat}}^* = \gamma_{\text{Lat}} = 0$. **c** Stiff surface: $k^*/k_c = 200$, interaction damping same as in **b**, no lateral forces. **d** The influence of the lateral forces and the inclination of the cantilever; thin solid line: $k^*/k_c = 200$, $k_{\text{Lat}}^* = \gamma_{\text{Lat}} = \alpha_0 = 0$; thick solid line: $k_{\text{Lat}}^* = 0.85k^*$, $\alpha_0 = 0$; dashed line: $\alpha_0 = 15^\circ$

due to lateral stiffness and inclination seem low, they can exceed the change in resonance frequency which would be expected from different materials, for example gold and steel.

The damping of the cantilevers is caused by two very different effects. System damping, which is caused by internal losses in the cantilever and by the surrounding air, affects all length elements of the beam in the same way. The tip-sample damping is localized to the end elements of the beam. Therefore, modes with high velocities at $x = L$ are more affected by tip-sample damping than others. Each mode has a different sensitivity not only to the interaction stiffness k^* but also to the tip-sample damping [14]. In the FMA the fundamental difference between system damping and interaction damping cannot be expressed because the two sources of damping are represented as two dashpots in series; therefore the time responses of the beam and the point-mass to a pulse excitation are fundamentally different [14].

2 Nonlinear response

In order to examine the effects of the higher modes on the nonlinear response, a suitable nonlinear interaction force curve $F(z)$ was composed of three analytical parts, representing a contact force, an exponential attractive intermediate force and a water-film force [15]. The nonlinear response

of the cantilever was calculated using the finite difference method [14]. It was assumed that the beam was initially in contact with the sample surface, deflected several nm according to a slight repulsive contact force. The specimen surface was then excited by a variable amplitude harmonic wave with $\omega = 2.0$ MHz shown as an inset in Fig. 4a. The excitation was ramped linearly in 20 cycle intervals, held at a constant amplitude of 1 nm for 20 cycles and then ramped back to zero. Figure 4 is a comparison between the beam model (b) and the point-mass model (a) for the nonlinear interaction force. The main difference that should be noted is the drastic difference in the high-frequency components of the vibration. The point-mass model neglects these higher modes even though they are seen to play a major role in the dynamics of the beam excited above the first resonance. The d.c. component prediction of the point-mass model, shown as the mean response in the inset of Fig. 4b, is qualitatively similar, although quantitatively different.

3 Conclusions

The high-frequency response of atomic force microscope cantilevers was examined using the elastic beam model and compared with solutions from the point-mass model. Important differences in the linear behavior of the two systems were

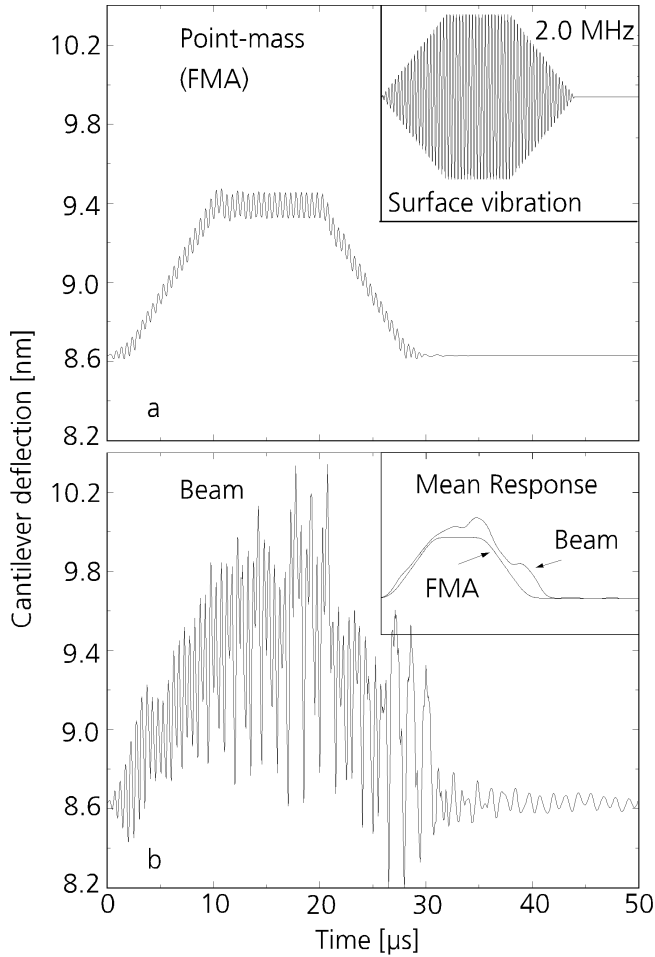


Fig. 4a,b. Nonlinear response of the cantilever to a tone-burst signal with variable amplitude, shown as an inset in **a**. High-frequency components of the cantilever vibration are missing in the signal calculated from the point-mass model (**a**) in comparison with the result from the beam model **b**. The mean response calculated from the two models is shown in the inset in (**b**)

found whenever the excitation frequency was near to or above the natural frequency of the first flexural mode. As a consequence of the difference in drive-point impedance, the effects of interaction stiffness and interaction damping are distinctly different in these two systems. The influence of the lateral tip-sample force and the difference between the amplitude and the slope at the end of the beam, which cannot be modeled by a point-mass, were shown to be considerable. Finally, a direct numerical simulation of the elastic beam equation, taking into account nonlinear forces, provided insight into the importance of the higher-order modes.

Acknowledgements. This work was partially supported by grants from the Volkswagen Foundation and the European Capital and Mobility program. The Alexander von Humboldt Foundation is gratefully acknowledged for their support of one of the authors (J.A.T.).

Appendix

Here we consider the situation where vibrations are forced in the cantilever by vibrating the clamped end at $x = 0$ with the amplitude $a(t) = a_0 e^{i\omega t}$. When the time dependencies are

omitted the boundary conditions for the tilted cantilever, taking into account lateral stiffness and damping are:

$$\begin{cases} y = a_0 & \text{at } x = 0, \quad \text{and} \\ \frac{\partial y}{\partial x} = 0 & \text{at } x = 0, \quad \text{and} \\ \begin{cases} \frac{\partial^2 y}{\partial x^2} = -T(k) \frac{\partial y}{\partial x} - X(k)y \\ \frac{\partial^3 y}{\partial x^3} = U(k)y + X(k) \frac{\partial y}{\partial x} \end{cases} & \text{at } x = L, \end{cases} \quad (\text{A.1})$$

where

$$T(k) = \frac{h^2}{L^3} \phi(k) \cos^2 \alpha_0 + \frac{h^2}{L^3} \phi_{\text{Lat}}(k) \sin^2 \alpha_0, \quad (\text{A.2})$$

$$X(k) = \frac{h}{L^3} \sin \alpha_0 \cos \alpha_0 (\phi(k) + \phi_{\text{Lat}}(k)), \quad (\text{A.3})$$

$$U(k) = \frac{1}{L^3} \phi(k) \sin^2 \alpha_0 + \frac{1}{L^3} \phi_{\text{Lat}}(k) \cos^2 \alpha_0. \quad (\text{A.4})$$

k is the wavenumber related to ω by the dispersion relation (2). $\phi(k)$ and $\phi(k)_{\text{Lat}}$ are functions containing the vertical and lateral contact stiffness and the vertical and lateral interaction damping, respectively:

$$\phi(k) = 3 \frac{k^*}{k_c} + i(kL)^2 p \quad p = \frac{3\gamma_{\text{int}}}{\omega_0 m^* (k_1 L)^2} \quad (\text{A.5})$$

$$\phi(k) = 3 \frac{k_{\text{Lat}}^*}{k_c} + i(kL)^2 p_{\text{Lat}} \quad p_{\text{Lat}} = \frac{3\gamma_{\text{Lat}}}{\omega_0 m^* (k_1 L)^2} \quad (\text{A.6})$$

p and p_{Lat} are dimensionless damping constants and $k_1 L \approx 1.875$ is the wavenumber times the length of the beam of the first free flexural mode. The response of the cantilever to the forcing can be calculated by inserting a general solution of the equation of motion (1) into the boundary conditions (A.1). The results are the following analytical expressions for amplitude and the slope at the end of the beam:

$$y(L, k) = \frac{a_0}{N(k)} \left(k^4 (\cos kL + \cosh kL) + k^3 T(k) (\sin kL + \sinh kL) - k^2 X(k) (\cos kL - \cosh kL) \right) \quad (\text{A.7a})$$

and

$$\alpha(L, k) = \frac{a_0 k}{N(k)} \left(k^4 (\sinh kL - \sin kL) - k^2 X(k) (\sin kL + \sinh kL) + k^2 U(k) (\cos kL - \cosh kL) \right) \quad (\text{A.7b})$$

with:

$$\begin{aligned} N(k) = & k^4 (1 + \cos(kL) \cosh(kL)) & (\text{A.7c}) \\ & + k^3 T(k) (\sin(kL) \cosh(kL) + \sinh(kL) \cos(kL)) \\ & + 2k^2 X(k) \sin(kL) \sinh(kL) \\ & + kU(k) (\sin(kL) \cosh(kL) - \sinh(kL) \cos(kL)) \\ & + (T(k)U(k) - X^2(k)) (1 - \cos(kL) \cosh(kL)) \end{aligned}$$

$y(L)$ and $\alpha(L)$ are complex amplitudes due to the complex representation of damping. The amplitude of vibration is the absolute value of the complex quantities, which was calculated with Mathematica [16].

References

1. G. Binnig, C.F. Quate, Ch. Gerber: Phys. Rev. Lett. **56**, 930 (1986)
2. G.M. McClelland, R. Erlandsson, S. Chiang: Rev. Progr. Quantitative Non-destructive Evaluation **6B**, 1307 (1987)
3. R. Wiesendanger, H.-J. Güntherodt (Eds.): Springer Series in Surface Sciences 28, *Scanning Tunneling Microscopy II* (1992); Springer Series in Surface Sciences 29, *Scanning Tunneling Microscopy III* (Springer, Heidelberg 1993)
4. V.B. Elings, J. Gurley: U.S. Patent No. 5.266.801 (1993)
5. P. Maivald, H.J. Butt, S.A. Gould, C.B. Prater, B. Drake, J.A. Gurley, V.B. Elings, P. Hansma: Nanotechnology **2**, 103 (1991)
6. K. Yamanaka, H. Ogiso, O. Kolosov: Appl. Phys. Lett. **64**, 178 (1994)
7. U. Rabe, W. Arnold: Appl. Phys. Lett. **64**, 1493 (1994)
8. B. Cretin, F. Sthal: Appl. Phys. Lett. **62**, 829 (1993)
9. W.F. Stokey: Vibration of systems having distributed mass elasticity, in *Shock and Vibration Handbook*, ed. by C.M. Harris, C.E. Crede (McGraw-Hill, New York 1976)
10. U. Rabe, K. Janser, W. Arnold: Rev. Sci. Instrum. **67**, 3281 (1996)
11. U. Rabe: Dissertation, Universität des Saarlandes, Saarbrücken (1996), unpublished
12. K.L. Johnson: Contact Mechanics (Cambridge University Press, Cambridge 1985)
13. P.-E. Mazeran, J.-L. Loubet: Tribol. Lett. **3**, 125 (1997)
14. J.A. Turner, S. Hirsekorn, U. Rabe, W. Arnold: J. Appl. Phys. **82**, 966 (1997)
15. S. Hirsekorn, U. Rabe, W. Arnold: Nanotechnology **8**, 57 (1997)
16. S. Wolfram: *Mathematica, a System for Doing Mathematics by Computer* (Wolfram Research Inc., 100 Trade Center Drive, Champaign, Illinois, 61820-7237 USA)